한국동력기계공학회지 제11권 제1호 pp.82~91 2007년 2월

Self-Sustained Tone Simulations using the Finite Difference Lattice Boltzmann Method with Flexible Specific Heat Ratio
조정 가능한 비열비를 갖는 FDLBM에 의한 자려발생 음의 시뮬레이션

S. K. Oh, S. W. Ahn, J. W. Kim and H. K. Kang*

Key Words : Aerodynamic Sounds, Finite Difference Lattice Boltzmann Method (FDLBM), Flexible Specific Heat Ratio, EdgeTone, Feedback Loop

Abstract : 기존의 2차원 FDLB 모델(D2Q21)에서 비열비 γ 는 공간의 차원수(D)에 의존한다. 즉, 2차원 공간의 계산에서는 $\gamma=(D+2)/D=2.0$밖에 취할 수 없으며, 공기와 같은 실체기체를 전산모사 하기에는 여러 어려움이 있다. 이러한 이유 때문에 문헌[1]의 LBM에서 제안된 조정 가능한 비열비 모델을 2차원 FDLB모델에 적용하여 자려발생 에지톤(edgetone)의 수치계산이 수행되었다. wedge의 선단각도가 $\alpha=23^0$(Case I) 및 20^0(Case II)를 갖는 2가지 모델이 설정되었으며, 노즐출구에서 wedge선단까지의 거리 w/d는 $3d\sim12d$사이에서 주어졌다. edgetone은 노즐로부터 나온 분류와 edge의 상호작용으로 이난 음압(sound pressure)의 차에 의해서 소음이 발생하며, 이 음압은 다시 상류의 분류에 영향을 미쳐 분류의 변동을 가져온다. w/d가 $9d$이하인 경우, 피드백(feedback) 메커니즘에 기인한 주기적인 운동이 발생하지만, w/d가 큰 $9d$이상인 경우에는 분류의 불안정성 때문에 규칙적인 분류의 운동은 보이질 않으며, 이는 기존의 연구결과들과 잘 일치함을 보였다.

본 연구에서 적용된 모델을 이용하여 공기와 같은 2원자 기체의 비열비 $\gamma=1.4$를 갖는 유체에 있어서 공력소음의 수치예측이 가능하다는 것을 확인하였다.

1. Introduction

As a relative new numerical method, the lattice Boltzmann (LBM)[2 4], a novel kinetic-based approach for simulating fluid flows and associated transport phenomena, has been successfully applied since it was developed from the lattice gas cellular automata method (LGCA)[5,6]. Considered an attractive alternative to conventional finite difference schemes because it recovers the Navier-Stokes equations, the LBM is computationally more stable, and easily parallelizable.

In traditional numerical methods, the macroscopic variables are obtained by solving the Navier-Stokes equations. But the LBM solves the microscopic kinetic equation for particle distribution function from which the particle move at unit speed on a regular grid subject to particle movement and simplified collision rules which conserve the total fluid mass, momentum and energy. The present method uses regularly space lattice, and particles residing on the lattice are replaced by the corresponding distribution functions and the collision operator is approximated by the BGK assumption. It could be considered as a special finite difference scheme of the continuous Boltzmann equation on a regular lattice[3], which also defines the associated discrete particle velocities. Therefore, discretization for the particle velocity can be decoupled from the spatial discretization, since the particle velocity in the Boltzmann equation is independent of the particle position.[7] This implies that this method can discretize the continuous velocity space into a set of discrete velocities with sufficient symmetry, while the usual spatial space may be discretized in some curvilinear coordinates.

접수일 : 2007년 12월 7일, 채택확정 : 2007년 1월 19일
강호근(책임저자) : 경상대학교 해양산업연구소
E-mail : kanghokeun@chol.com Tel. 055-640-3064
오세경, 안수환 : 경상대학교 기계항공공학부
김정환 : 조선기자재연구원

Meanwhile, the numerical solution of flow acoustic problems at relatively low Mach number flow conditions ($Ma \leq 0.3$) still is a major problem, which is often seen in various fields of industry. For instance prediction and reduction of aerodynamic sound is as important as improvement in aerodynamic performance for further speed-up of present high-speed vehicles since it dominates the overall sound that is generated from such vehicles. So, the finite difference-based LBM (FDLBM) seems the most promising method that computes source fluctuations in the flow for the prediction of aerodynamic sounds and at the same time prediction of aerodynamic sound seems to be one of the most appropriate areas of engineering applications of LBM. In the field of aerodynamic sounds some fundamental studies has been undertaken showing its validity concerning linear and nonlinear wave propagation[8], acoustical streaming[9] and aeolian tonal.[10] So the use of the LBM or FDLBM as a tool for computational aerodynamic sounds can be seen as in its early stage.

Most models in LBM or FDLBM is for incompressible fluids due to its simplicity of the structure, and only a few simulations by the models for compressible or thermal-fluid model [2,11] have been reported. In LBM, the mode of energy of the fluid particle is limited to that due to translation. Then the ratio of the specific heats is

$$\gamma = (D+2)/D \tag{1}$$

where D represents the space dimension. For the case of 2-dimensional, the ratio of specific heat is $\gamma = 2.0$, and it will be applicable to monatomic gases only but not to the most important diatomic gas such as an air.

The overall purpose of this paper is, based on detailed comparisons with the experimental and numerical data, to demonstrate the capability of FDLB model with flexible specific heat ratio γ and acoustical simulations for the prediction of sound that is generated from with a relatively low Mach number. Our simulations deals with Reynolds numbers, $200 \leq Re \leq 600$ and $0.027 \leq S_d \leq 0.077$, respectively.

The governing equations and numerical method for the FDLBM of compressible fluid model will be presented in Section 2. The accuracy of the FDLB model with flexible specific heat ratio γ will be validated in Section 3. Section 4 will explained the predictions of edgetone in two different cases including prediction of the far-field sounds as a benchmark problems. In Section 5, conclusions will be summarized.

2. Computational methodology

2.1. Finite difference lattice Boltzmann method

The Boltzmann equation to be solved is the following discretized Bhatnager-Gross-Krook (BGK) equation as:

$$\frac{\partial f_i}{\partial t} + c_{i\alpha}\frac{\partial f_i(t,\mathbf{r})}{\partial r_\alpha} = -\frac{1}{\phi}\left[f_i(t,\mathbf{r}) - f_i^{(0)}(t,\mathbf{r})\right] \tag{2}$$

where, the real number f_i is the normalized number of particles at each node $\mathbf{r}$ and time t, moving direction i and α the Cartesian coordinates, $f_i^{(0)}$ on the RHS is the local equilibrium distribution function, and ϕ is call the single relaxation time factor.

In equation (2), the relationship between the relaxation time ϕ and the kinetic viscosity μ is given as,

$$\mu = \frac{2}{D}\rho e \phi \tag{3}$$

where ρ is density and e the internal energy per unit mass. Here the stability criterion of the collision term in RHS of Eq.(2) demands that the time increment $\Delta t < \phi/2$, if we use the first order Euler scheme for the time integration. Therefore, the time increment must be very small for high Reynolds number flow and calculation efficient will be poor.

In order to apply for high Reynolds number and speed up the calculation time, the modified

equation by Kang and Tsutahara[10] in which the third term is added to the discretized BGK equation (Eq.(2)) is transformed as:

$$\frac{\partial f_i}{\partial t}+c_{i\alpha}\frac{\partial f_i(t,\mathbf{r})}{\partial r_\alpha}-\frac{Ac_{i\alpha}}{\phi}\frac{\partial(f_i-f_i^{(0)})}{\partial r_\alpha} =-\frac{1}{\phi}\left[f_i(t,\mathbf{r})-f_i^{(0)}(t,\mathbf{r})\right] \tag{4}$$

in which $A(>0)$ is a constant, and other variables are the same as in Eq.(2).

2.2 A model having flexible specific heat ratio

We propose a model having energy modes except the translation $G_i(t,\mathbf{r})=f_i(t,\mathbf{r})E_i(t,\mathbf{r})$ to give the particle internal degree of freedom, which was proposed by Takada and Tsutahara[1] in LBM. The distribution function $G_i(t,\mathbf{r})$ is supposed to approach by collisions to its local equilibrium state $G_i^{(0)}=f_i^{(0)}E_i^{(0)}$ as the particle distribution functions do, and the evolution of $G_i(t,\mathbf{r})$ is transformed as

$$\frac{\partial G_i}{\partial t}+c_{i\alpha}\frac{\partial G_i(t,\mathbf{r})}{\partial r_\alpha}-\frac{Ac_{i\alpha}}{\phi}\frac{\partial(G_i-G_i^{(0)})}{\partial r_\alpha} =-\frac{1}{\phi}\left[G_i(t,\mathbf{r})-G_i^{(0)}(t,\mathbf{r})\right] \tag{5}$$

Here, assumed that all the particles at the local equilibrium stage have the same rotation energy as:

$$G_i^{(0)}=Ef_i^{(0)} \tag{6}$$

$$E=\frac{D}{2}\left(\frac{D+2}{D}-\gamma\right)e \tag{7}$$

The local equilibrium distribution function can be defined as

$$f_i^{(0)}\cong F_i\rho[1-2Bc_{i\alpha}u_\alpha+2B^2(c_{i\alpha}u_\alpha)^2+Bu_\alpha u_\beta -\frac{4}{3}B^3(c_{i\alpha}u_\alpha)^3-2B^2c_{i\alpha}u_\alpha u_\beta u_\gamma] \tag{8}$$

in which the subscript α represents Cartesian coordinates. The constants F_i and B are explained in ref.[10]. Then the expression for the ratio of the specific heats γ in Eq.(1) will be written as

$$\gamma=\frac{D+2}{D^*}=\frac{D+D_E+2}{D+D_E} \tag{9}$$

where D^* is the total degree of freedom of the particle motion and D_E is the degree of freedom of the rotation. Therefore, the ratio of the specific heats γ can be freely variable to $1.0<\gamma\le 2.0$ for 2-dimensional model.

3. Verification of accuracy

In order to validate the applicability of the present algorithm to acoustics, we consider a weak propagating tube flow as shown in Fig.1, with the size 1.0×0.05 (400×100 cells). The pressure distribution is also illustrated. The rectangular channel is a device in which weak normal propagating waves are generated by the rupture of a diagram initially separating a high pressure gas from the low pressure gas. After the rupture of the diagram, the system eventually approaches to an equilibrium state, with the final state of the closed-end tube determined from the first law of thermodynamics. Here, of primary interest is not the final equilibrium state of the gas, but the transient weak wave phenomena occurring immediately after the rupture of the diagram.

The pressure ratio p_1/p_2 is 1.0×10^6 and is so small that linear compression and expansion waves propagates at the sound speed, where specific heat ratio γ=1.4, internal energy e=0.5 and time increment $\Delta t=2.0\times10^{-3}$. In Fig. 2, the sound speed simulated by the model of the flexible specific heat ratio is compared to the theoretical value as well as MacCormac scheme. As shown in figure, it is confirmed that the FDLBM with the third-order upwind scheme shows in much better agreement with the theoretical prediction than that of second order upwind scheme as well as MacCormac method, suggesting that the model is able to handle very small pressure oscillations occurring in aerodynamic problems.

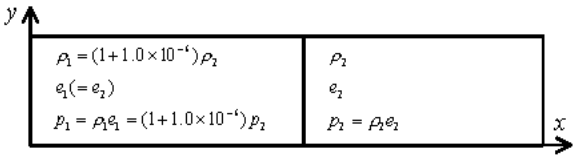

Fig. 1 Calculation condition

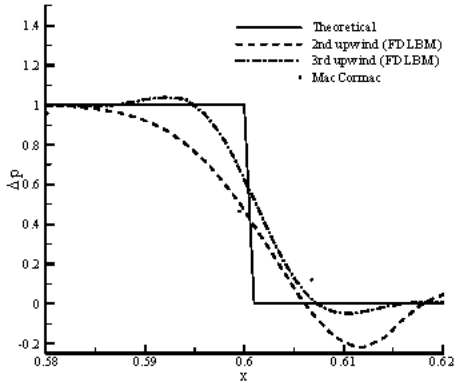

Fig. 2 Comparison of theoretical, MacCormac and FDLBM

4. Edgetone

Edgetone is a discrete frequency sound produced by several flow geometries in which a free shear layer interacts with a solid boundary. The sound is generated because the impinging jet forms a self excited flow maintained by a feedback loop. Particularly obvious are the main features by the simplifying considerations first stated by Powell.[12]

A perturbation of the jet with speed U finally results in a vortex further downstream. It travels with a phase velocity c_p and encounters the edge at the stand-off distance w. Here the vortex interacts and radiates an acoustical wave feeding back upstream to the region of the flue. Then the oscillatory behaviour with the frequency f is related the phase velocity of both, the acoustical wave c_0 as well as the perturbation. Such a feedback theory was proposed by Rossiter[13] in the following form,

$$\frac{w}{c_p}+\frac{w}{c_0}=\frac{k}{f},\quad k=1,2,3,\cdots \tag{10}$$

where k is constant for a stage. From experiments it appears that k has to be replaced by $(k-\beta)$, β being a phase offset. As a result the above relation would yield

$$S_w=(k-\beta)/(U/c_p+Ma) \tag{11}$$

where $Ma=U/c_0$ is the Mach number. In our case c_0 is much larger than c_p. Typical values for c_p/U are between $0.4\sim0.6$. Our interest in this research is focused on the stage I, or the fundamental fluid dynamical mode $k=1$

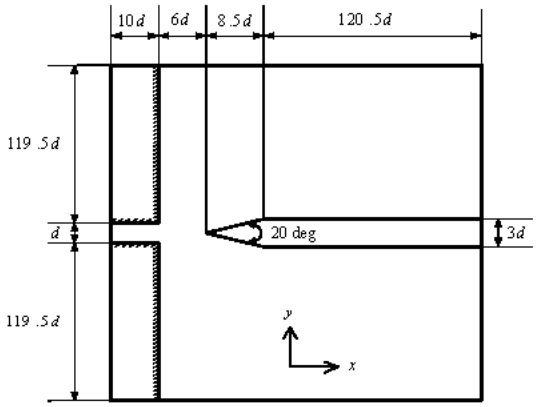

(a) Case I

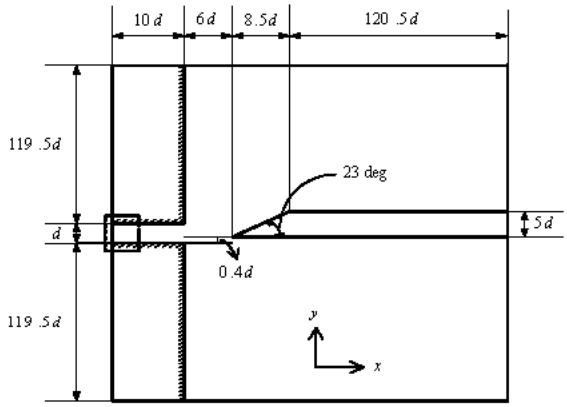

(b) Case II

Fig. 3 Edgetone geometries for w/d=6

More recently, the theoretical developments performed by Holger et al.[14] and Howe[15] have confirmed the analogy. Several scaling laws derived from experimental or theoretical work have also been proposed to fit the dependency of the oscillation frequency f on the parameter d/w, where d is the nozzle height and w denotes the stand-off distance between the nozzle outlet and

the wedge. These authors proposed the following more general law in term of the Strouhal number S_d for $k=1$:

$$S_d = f \cdot d/U_0 = C \cdot (d/w)^n \quad (12)$$

where n equals 3/2 for the w dependence, and U_0 the maximum velocity at the nozzle exit. In general the constant C might depend also the Reynolds number. In former experiments n was shown to be between 1 and 3/2, depending on the experimental configuration. There are two explanations for a behaviour with $n>1$ depending on the state of turbulence of the jet. At low Reynolds numbers the flow is pseudo-laminar. As will be argued below, the phase velocity can be derived from linear instability theory through dispersion relations. From this, its frequency dependence results in $n \approx 1$.

4.1 Numerical conditions

The edgetone configurations considered consist of sharp edge tip located in the medial plane of a fully developed two-dimensional jet as shown Fig. 3. The height of the nozzle and the shape of the edge are similar to those of Brown's work[16] and Bamberger's work[17]. Especially, Brown has performed detailed experiments regarding the edgetone and obtained the following equation.

$$f = 0.466k(U-40)\left[\frac{1}{w}-0.07\right] \quad (13)$$

where f is the frequency with k=1.0, 2.3, 3.8 and 5.4 for the four stages respectively.

The thickness of the models is 1 (mm) and all the length scales are normalized by the height of nozzle d in the computations. Computational domains are set for $-10d \le x \le (132d \sim 141d)$ and $-120 \le y \le 120d$ for each case, and the edges are composed of angle of attack $\alpha = 20^0$ (Case I) and 23^0(Case II), respectively. The grids are clustered at the edge walls. For spatial derivatives, a third-order upwind scheme is employed and a second-order Runge-Kutta scheme is used for time integration. A parabolic inflow profile for the velocity is prescribed on the inflow boundary. Adiabatic and no-slip conditions are employed on the wedge and walls, and outflow is imposed on the outer far field boundary. Table 1 shows the calculation conditions for each case.

Table 1 Calculation conditions

	w/d	cells	domains	variables
case I	3d	331×381	-10d<x<132d -120d<y<120d	Re=250~600 Δt=0.01 γ=1.4 20℃ air
	6d	361×381	-10d<x<135d -120d<y<120d	
	9d	397×381	-10d<x<138d -120d<y<120d	
	12d	433×381	-10d<x<141d -120d<y<120d	
case II	3d	266×301	-10d<x<132d -120d<y<120d	
	6d	301×301	-10d<x<135d -120d<y<120d	
	9d	321×301	-10d<x<138d -120d<y<120d	
	12d	341×301	-10d<x<141d -120d<y<120d	

4.2 Evaluation and comparison

The Stouhal numbers are plotted in Fig. 4 as a function of ratio w/d. Our simulations deal with moderate Reynolds number, Re=250~600 and Strouhal numbers $0.027 \le S_t \le 0.077$. Hence, rather the situation $n \simeq 1$ is expected. Three values of the stand-off distance w are considered (6, 9 and 12 mm), and the results obtained at frequency levels 1 are reported. The present calculations are compared to the experimental and numerical ones obtained previously in similar flow configurations.[16 19] The theoretical law of Eq.(12) with $C=0.92(k+0.4)$ proposed by Holger et al.[14] is also presented in Fig.3 for frequency levels k=1 and 2. In current results, the reliable agreement is found between experimental, numerical and theoretical results concerning the Strouhal number S_t.

The first level frequencies are obtained in the simulations by analyzing the time evolution of the far-field pressure. Then the Strouhal numbers predicted by the simulations are plotted in Fig. 5 for different Reynolds numbers ranging from 150 to 600, for each type of injected air. A good agreement by Devillers and Coutier-Delgosha[19] is found in the whole range of Reynolds number. The discrepancy is lower than 6.5 % under Re=500 in all cases.

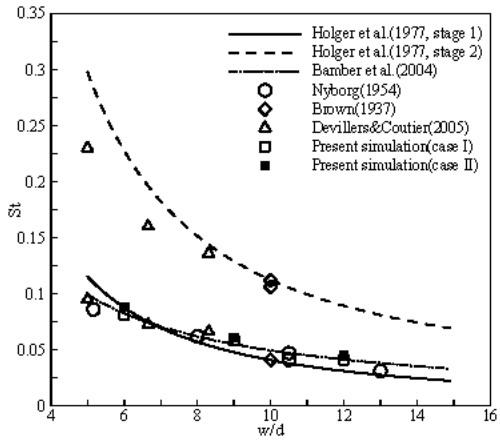

Fig. 4 Comparison of the Strouhal numbers with FDLBM, experiments and theoretical results (frequency stages 1 and 2)

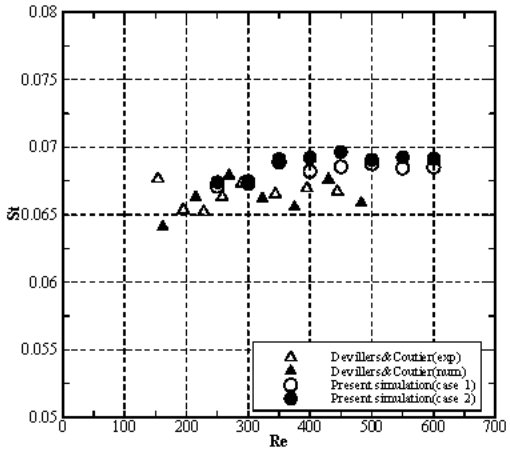

Fig. 5 Comparison between FDLBM and the results by Devillers and Coutier-Delgosha[19] (stage I)

4.3 Feedback loop

In the near-field flow structure, instantaneous vorticity for two different cases with w/d=6 are presented in Figs. 6 and 7. The initial values are given at U_0=12 m/s, Re=600 and γ=1.4. A jet

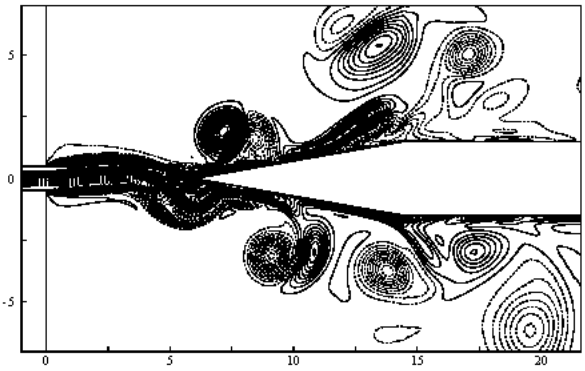

(a) T=450

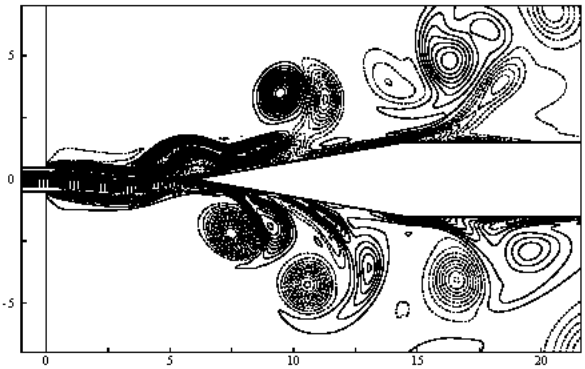

(b) T=458

Fig. 6 Instantaneous vortex distribution for case I.

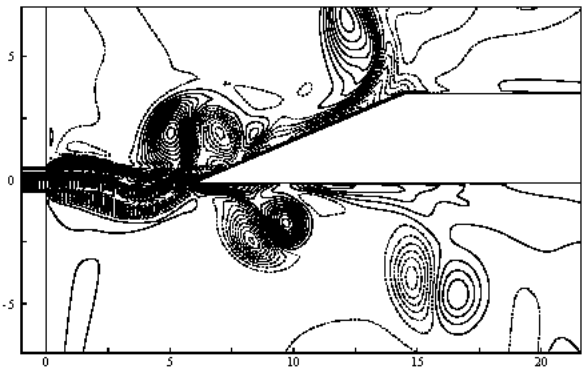

(a) T=460

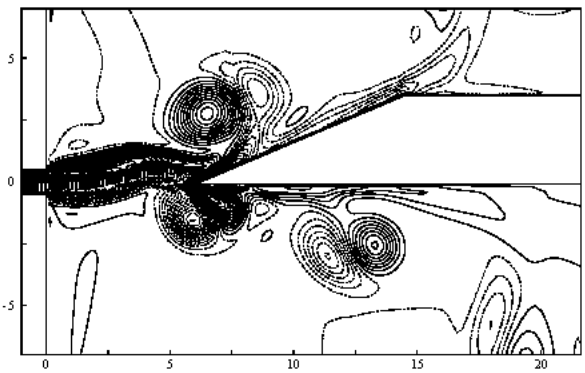

(b) T=468

Fig. 7 Instantaneous vortex distribution for case II.

which comes out of the nozzle first collides with the edge, and then the jet begins to fluctuate. This fluctuation synchronizes with the period of the vortex, which arises from the top and bottom wall in the vicinity of the nozzle exit. It is considered that, because of the vortex, the fluctuation of the jet is induced. Then with the effect of the jet, the vortex moves toward downstream, and it undulates like the form of the jet by the rotation energy. As a result, the jet changes its direction(Fig. 6(a)→(b) or Fig.7(a)→(b)) due to the rotation of the vortex in the vicinity where the vortex exceeded the tip of the wedge, and flows into unilateral sides of the wedge. In the real flow the vortices do not persist far downstream and decay.

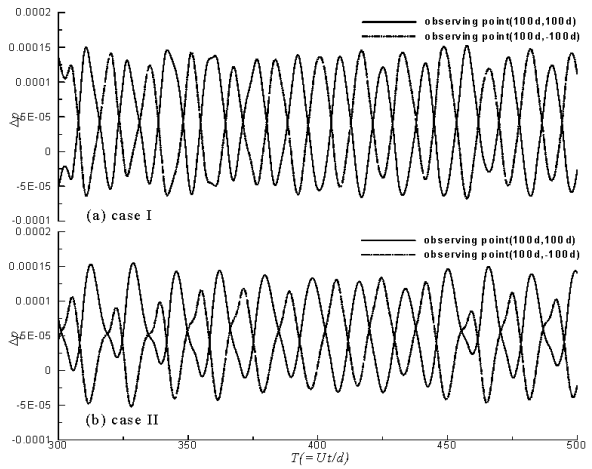

Fig. 8 Time variations of acoustic pressure for each case.

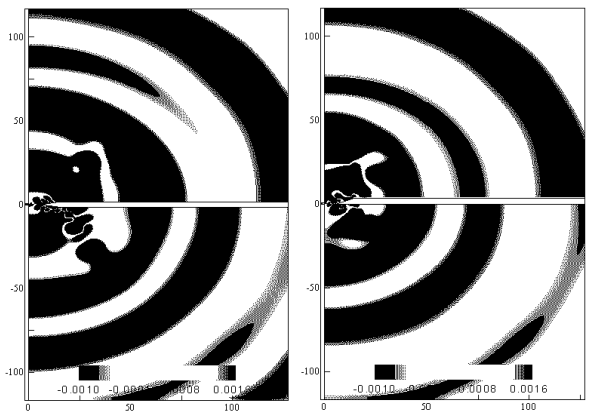

(a) case I (b) case II

Fig. 9 Edgetone (-0.001≤△p≤0.0016): (a) T=450; (b) T=460.

The time variations of the acoustic pressure measured at two points are shown in Fig.8 for the case of U_0=12 m/s, respectively. The acoustic pressure $\triangle p$ is defined as

$$\triangle p = (p - p_0)/p_0 \tag{14}$$

The observing points are radically considered on the edge tip (x_0, y_0), in which these points apart from $(100d, \pm 100d)$ in x and y direction. The sound signals fluctuate with a period of $\triangle t$=20.48 and 19.88, which corresponds to $S_t(=fd/u)$= 0.049 and 0.051, respectively. The acoustic pressure becomes periodic with maxima and minima occurring at points.

To examine the farfield acoustic pressure for the case of Ma=0.2 and Re=800, Fig. 9 shows the acoustic pressure field for two different instants, where the contour level $\triangle p_{step}$ fluctuates from -0.001 to 0.002. As can be seen these figures, rarefaction waves with negative $\triangle p$ and compression waves with positive $\triangle p$ are generated alternately around the edge tip at the origin, and propagate symmetrically in the upper and lower parts of the wedge.

4.4 Stand-off distance with periodicity

In this section we discuss the effect of stand-off distance between the nozzle exit and the wedge for w/d=3, 6, 9 and 12, respectively. Initial conditions are set Ma=0.2, Re=600 and γ =1.4, respectively, and all calculation conditions are the same in the case of previous section.

Figs. 10(a)-(d) and 11(a)-(d) show the instantaneous vorticity fields at t=465. For each case, it confirms that the blown jet oscillates at the upper and lower sides of the wedge, but the flow patterns are different from each case. For the case of stand-off distance w/d=3 and 6 in Figs. 10 (a), (b) and 11(a), (b), the jet oscillates in a periodic fashion, while for w/d=9 and 12 in Figs. 10(c), (d) and 11(c), (d) it also oscillates but the flows does not periodically. The greater w/d allows more jet pattern variation before

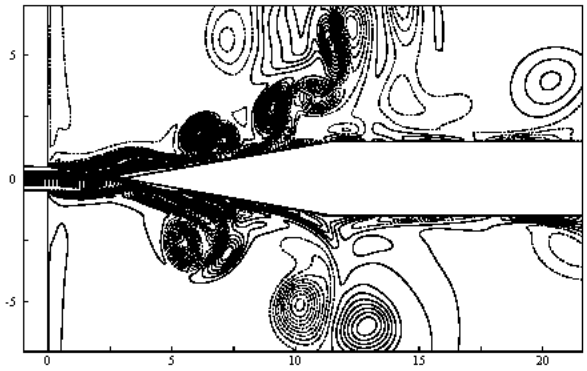

(a) w/d=3

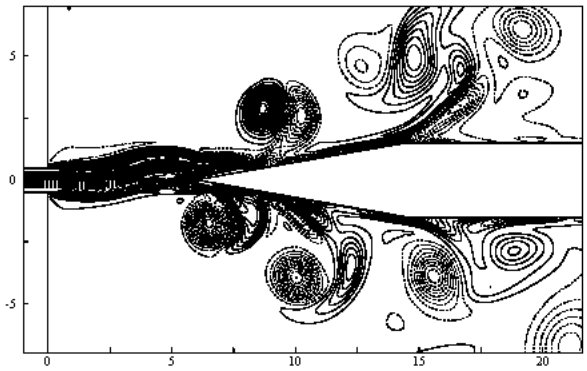

(b) w/d=6

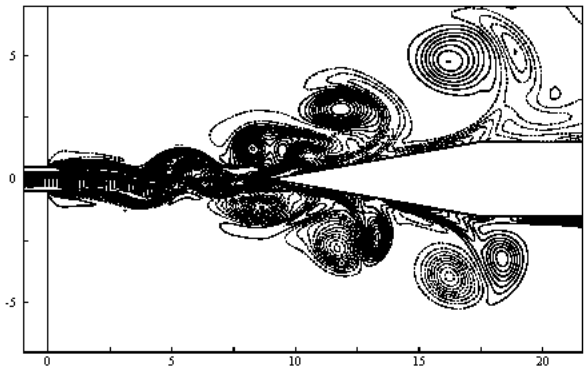

(c) w/d=9

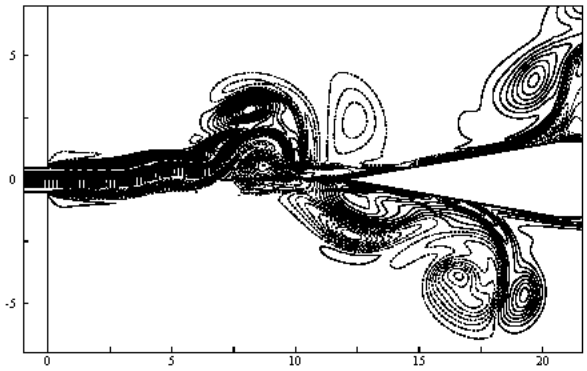

(d) w/d=12

Fig. 10 Instantaneous vortex distribution under various w/d for case I.

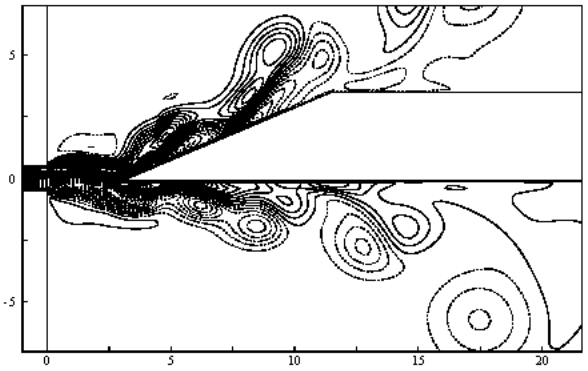

(a) w/d=3

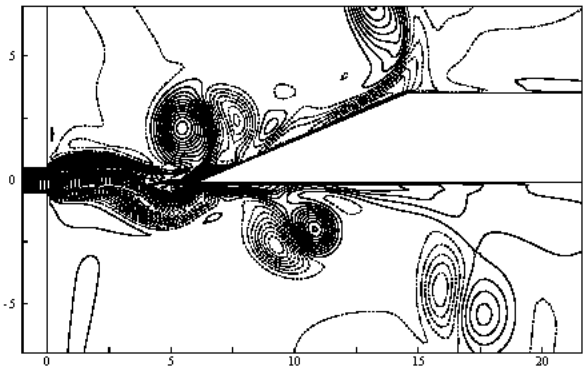

(b) w/d=6

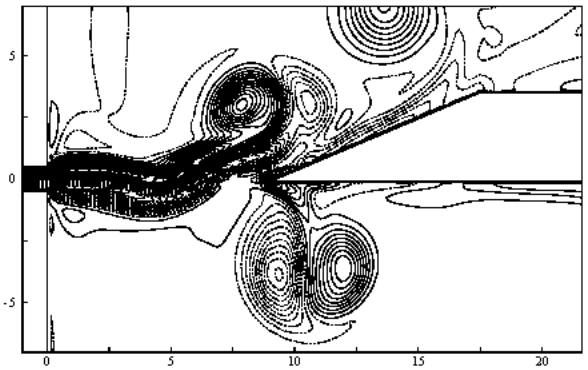

(c) w/d=9

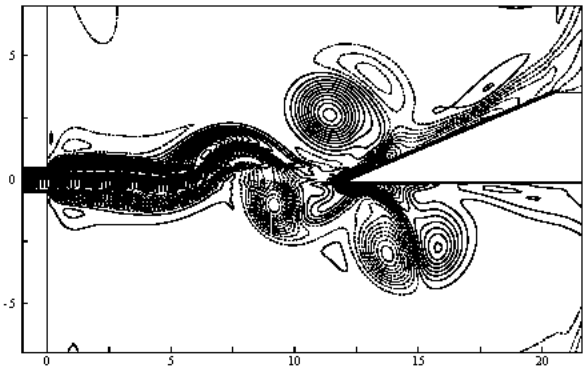

(d) w/d=12

Fig. 11 Instantaneous vortex distribution under various w/d for case II.

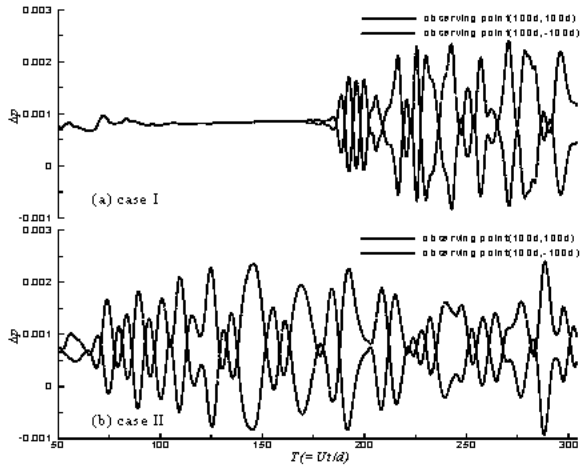

Fig. 12 Time variations of acoustic pressure for w/d=12.

interaction with the wedge. In case of w/d=12, figure 12 presents the acoustic signal measured at $(x,y)=(100d,100d)$ from the tip of the edge. In these figures when jet speed decreases as wedge distance increases, the jet is more susceptible to the wedge dipole effects, which deflect the jet and create vortex/undulation centers along the jet boundaries. Consequently, the jet exhibits the extremely dynamic nature of the edgetone flow field near the wedge apex. According to Brown's experiment[16], when the distance from the wedge to the nozzle exit is greater than w/d=20, the acoustic feedback, with strength decreasing linearly with distance, would be too weak to trigger alternate vortex shedding at the nozzle exit.

5. Conclusions

The ability of the FDLBM to produce aerodynamic sounds for relatively low Mach number flows ($Ma \leq 0.3$) which was introduced a lattice BGK model for 21 bits with flexible specific heat ratio, is validated in several examples. 2-dimensional edgetone phenomenon is successfully simulated by the applied FDLBM, agreed well with the other's experimental and numerical results.

The obtained results in this study show potentiality of FDLBM of aerodynamic sounds generated from arbitrary objects with complex shapes.

References

1. N. Takada and M. Tsutahara, 1999, "Proposal of Lattice BGK Model with Internal Degrees of Freedom in Lattice Boltzmann Method", Trans. JSME Journal, B, Vol. 65, No. 629, pp. 92-99.
2. F. J. Alexander, S. Chen and D. J. Sterling, 1993, "Lattice Boltzmann Thermodynamics", Physical Review E, Vol. 47, pp. 2249-2252.
3. X. Y. He and L. S. Luo, 1997, "Theory of the lattice Boltzmann method: from the Boltzmann equation to the lattice Boltmann equation", Physical Review E, Vol. 56, pp. 6811-6817.
4. Y. Chen and G. D. Doolen, 1998, "Lattice Boltzmann Method for Fluid Flows", Annual Review Fluid Mechanics, Vol. 30, pp. 329-364.
5. B. Chopard and M. Droz, 1998, Cellular automata modeling of physical systems, Cambridge University Press: Cambridge, MA.
6. D. A. Wolf-Gladrow, 2000, Lattice-gas cellular automata and lattice Boltzmann models: an introduction, Berlin Heidelberg, Springer-Verlag.
7. N. Cao, S. Chen, S. Jin and D. Martinez, 1997, "Physical Symmetry and Lattice Symmetry in the Lattice Boltzmann Method", Physical Review E, 55, pp. R21-R24.
8. J. M. Buick, C.L. Buckley, C. A. Greated and J. Gilbert, 2000, "Lattice Boltzmann BGK simulation of nonlinear sound waves: the development of a shock front", Journal of Physics A: Mathematical and General, Vol.33, pp.3917-3928.
9. D. Haydock and J. Yeomans, 2001, "Lattice Boltzmann simulations of acoustic streaming", Journal of Physics A, vol. 34, pp. 5201-5213.
10. H. K. Kang and M. Tsutahara, 2007, "An application of the finite difference-based lattice Boltzmann model to simulating

flow-induced noise", International Journal for Numerical Methods in Fluids, Vol. 53, pp. 629-650.

11. Y. Chen, H. Ohashi and M. Akiyama, 1994, "Thermal lattice Bhatnager Gross Krook model without nonlinear deviation in macrodynamic equations, Physical Review E, Vol.50, pp. 2776-2783.
12. A. Powell, 1953, "On the edge tone and associated phenomena", Acoustica 3, Vol. 3, pp. 233-243.
13. J. E. Rossiter, 1962, "The effect of cavities on the buffeting of the aircraft", Royal Aircraft Establishment Technical Memorandum 745.
14. D. K. Holger, T. A, Wilson and G.S. Beavers, 1977, "Fluid Mechanics of the Edgetone," Journal of Acoustical Society of America, Vol. 62(5), pp. 1116-1128.
15. M. S. Howe, 1998, Acoustics of fluid structure interaction, Cambridge University Press, Cambridge
16. G. B. Brown, 1937, "The vortex motion causing edge tones", Proceedings of the Physical Society of London, Vol. 49, pp. 493-507.
17. A. Bamber, E. Bansch and K. G. Siebert, 2004, "Experimental and numerical investigation of edge tones", ZAMM. Angew. Math. Mech., Vol. 84, No. 9, pp. 632-646.
18. W. Nyborg, 1954, "Self-maintained oscillations in a jet edge system", Journal of the Acoustical Society of America, Vol. 26, pp. 174-182.
19. J. F. Devillers and O. Coutier-Delgosha, 2005, "Influence of the Nature of the Gas in the Edge-tone Phenomenon", Journal of Fluids and Structures, Vol. 21, pp. 133-149.